Water Research 122 (2017) 139–147

Contents lists available at ScienceDirect

Water Research

journal homepage: www.elsevier.com/locate/watres

Biosorption of metal elements by exopolymer nanofibrils excreted from *Leptothrix* cells

Tatsuki Kunoh [a, b], Makoto Nakanishi [a, b], Yoshihiro Kusano [c], Atsushi Itadani [d, e], Kota Ando [e], Syuji Matsumoto [a, b], Katsunori Tamura [a, b], Hitoshi Kunoh [a, b], Jun Takada [a, b, *]

[a] Core Research for Evolutionary Science and Technology (CREST), Japan Science and Technology Agency (JST), Okayama 700-8530, Japan
[b] Graduate School of Natural Science and Technology, Okayama University, Okayama, 700-8530, Japan
[c] Department of Applied Chemistry and Biotechnology, Okayama University of Science, Okayama, 700-0005, Japan
[d] Department of Human Sciences, Obihiro University of Agriculture and Veterinary Medicine, Hokkaido, 080-8555, Japan
[e] Graduate School of Science and Technology, Niigata University, Niigata, 950-2181, Japan

ARTICLE INFO

Article history:
Received 24 January 2017
Received in revised form
2 May 2017
Accepted 3 May 2017
Available online 4 May 2017

Keywords:
Biosorption
Leptothrix
Sheath materials
Exopolymer fibrils
Sorbed metal elements
Amorphous organic–inorganic complex

ABSTRACT

Leptothrix species, aquatic Fe-oxidizing bacteria, excrete nano-scaled exopolymer fibrils. Once excreted, the fibrils weave together and coalesce to form extracellular, microtubular, immature sheaths encasing catenulate cells of *Leptothrix*. The immature sheaths, composed of aggregated nanofibrils with a homogeneous-looking matrix, attract and bind aqueous-phase inorganics, especially Fe, P, and Si, to form seemingly solid, mature sheaths of a hybrid organic–inorganic nature. To verify our assumption that the organic skeleton of the sheaths might sorb a broad range of other metallic and nonmetallic elements, we examined the sorption potential of chemically and enzymatically prepared protein-free organic sheath remnants for 47 available elements. The sheath remnants were found by XRF to sorb each of the 47 elements, although their sorption degree varied among the elements: >35% atomic percentages for Ti, Y, Zr, Ru, Rh, Ag, and Au. Electron microscopy, energy dispersive x-ray spectroscopy, electron and x-ray diffractions, and Fourier transform infrared spectroscopy analyses of sheath remnants that had sorbed Ag, Cu, and Pt revealed that (i) the sheath remnants comprised a 5–10 nm thick aggregation of fibrils, (ii) the test elements were distributed almost homogeneously throughout the fibrillar aggregate, (iii) the nanofibril matrix sorbing the elements was nearly amorphous, and (iv) these elements plausibly were bound to the matrix by ionic binding, especially via OH. The present results show that the constitutive protein-free exopolymer nanofibrils of the sheaths can contribute to creating novel filtering materials for recovering and recycling useful and/or hazardous elements from the environment.

© 2017 Published by Elsevier Ltd.

1. Introduction

Biosorption is a term used to describe the removal of heavy metals from an aqueous solution via their passive binding to a nonliving biomass, while the term bioaccumulation describes an active process whereby removal of the metals requires the metabolic activity of a living organism (Davis et al., 2003). Therefore, any removal that depends on the uptake of metals by living organisms for use as an energy source and essential element for their survival is categorized as bioaccumulation. Anthropogenic release of heavy or precious metals in environments is very frequently related to wastewaters discharged from industrial, mining and living activities (Cruz Viggi et al., 2010; Davis et al., 2003). For discovering the mechanisms of biosorption and/or bioaccumulation, a variety of techniques have been tested to recover various metal ions such as Ag(I), Au(III), Cr(VI), Cu(II), Fe(II), In(III), Ni(II), Pb(II), Pd(II), Pt(IV), Rh(III), U(VI), Re(VII), and Zn(II) from anthropogenic environments using diverse organisms such as brown algae, yeasts, and bacteria or their products (Cruz Viggi et al., 2010; Davis et al., 2003; Han et al., 2006; Pagnanelli et al., 2004; Raoa and Prabhakara, 2011; Zhao et al., 2016). A good example is the biogenic technology to recycle electrical wastes termed “urban mining” by which many useful precious metals are recovered (Bhat et al., 2012; Inoue et al.,

* Corresponding author. Graduate School of Natural Science and Technology, Okayama University, Okayama, 700-8530, Japan.
E-mail address: jtakada@cc.okayama-u.ac.jp (J. Takada).

http://dx.doi.org/10.1016/j.watres.2017.05.003
0043-1354/© 2017 Published by Elsevier Ltd.

2015).

Ocherous deposits or floats that are often seen in nearly neutral water of lakes, ponds, swamps, drainage ditches, and springs are known to be produced by biomineralizing Fe-/Mn-oxidizing bacteria that inhabit groundwater outwellings (Emerson et al., 2010; Ghiorse, 1984; Spring, 2006). The genus *Leptothrix*, a typical group of these bacteria, can produce extracellular and microtubular sheaths encrusted with Fe and/or Mn oxyhydroxides and Si, P, and sometimes Ca (Emerson et al., 2010; Furutani et al., 2011; Ghiorse, 1984; Spring, 2006). The basic skeleton of the sheaths, consisting of aggregated organic fibrils excreted from the bacterial cells, contain polysaccharides, proteins, and lipids with various functional groups (Chan et al., 2009; Emerson and Ghiorse, 1993a). The metal encrustation of the sheaths is considered to result from the interactions between such functional groups and aqueous-phase inorganics (Emerson and Ghiorse, 1993a; Furutani et al., 2011; Seder-Colomina et al., 2013; Takeda et al., 2005; Spring 2006). Indeed, a strong correlation exists between the presence of acidic polysaccharides with carboxyl groups and the distribution of iron oxyhydroxides in *Leptothrix* sheaths (Chan et al., 2009). Alternatively, Fe(III) particles that are abiotically generated in the medium adhere directly to the sheath materials, which consist of aggregated constitutive nanofibrils in culture (Kunoh et al., 2016a, b). Such direct adherence of the Fe(III) particles also occurs on cell- and protein-free sheath remnants that are enzymatically and chemically prepared from the sheaths (Kunoh et al., 2016a, b), providing evidence that the sorption potential of the sheath materials, at least partially, may be a case of so-called biosorption.

In addition to the reported studies describing high affinity of the *Leptothrix* sheaths for a variety of metal cations such as Zn and Pb (Boonfueng et al., 2009; Nelson et al., 1999, 2002), earlier papers on the mode of metal encrustation of the sheaths (Chan et al., 2009; Emerson and Ghiorse, 1993a; Furutani et al., 2011; Seder-Colomina et al., 2013; Spring 2006; Takeda et al., 2005) led us to assume that the basic organic skeleton of the sheaths may have a fundamental sorption potential for various metallic and nonmetallic cationic ions, which may lead to the development of novel filter materials to recover precious and/or hazardous cations from aquatic environments.

In this study, we examined the sorption potential of enzymatically and chemically prepared sheath remnants against a variety of metallic and nonmetallic elements by using x-ray fluorescence (XRF) and diffraction (XRD) assays and imaging and element distribution analyses with high angular annular dark-field (HAADF) electron microscope, energy-dispersive x-ray spectrometer (EDX), electron diffraction (ED), and Fourier transform infrared spectroscopy (FT-IR).

2. Materials and methods

2.1. Strain, medium, and culturing

Leptothrix cholodnii strain SP-6 (ATCC 51168) was transferred from frozen stock onto MSVP agar (Emerson and Ghiorse, 1992) with sterile toothpicks, followed by incubation at 20 °C for 4–5 days. Single colonies were then transferred to 25 mL of MSVP broth with sterile toothpicks and incubated on a rotary shaker (EYELA FMC-1000, Tokyo Rikakikai, Tokyo, Japan) at 22 °C and 70 rpm. After 2–3 days, 10–25 mL of the preculture was transferred to 100–500 mL of MSVP broth in glass flasks and incubated for 2–3 more days. Formation of the immature sheaths was confirmed by differential interference microscopy, as reported previously (Kunoh et al., 2016a, b). The skeleton of an initial sheath (30–50 nm thick in 2 day culture), consisting of organic exopolymer fibrils of bacterial origin, is formed first, then the sheath becomes encrusted with aquatic inorganics (Ishihara et al., 2013). We designate such an initial sheath before sufficient metal encrustation as an immature sheath in this study. The bacterial cells and associated immature sheaths were collected by centrifugation and repeatedly washed with ultrapure water (UPW) and then used to prepare cell-free and protein-free sheath remnants.

2.2. Preparation of cell-free and protein-free sheath remnants

For obtaining cell-free sheath remnants, the sheath specimens were treated with lysozyme/EDTA/SDS as reported previously (Emerson and Ghiorse, 1993a; Kunoh et al., 2016a, b) (hereafter referred to as LES treatment). Briefly, specimens from 4 to 6 L of culture were washed once in UPW and suspended in 22.5 mL of lysis solution containing 2.5 mM EDTA and 150–500 μg of lysozyme (Sigma-Aldrich, St. Louis, MO, U.S.A.). After the reaction mixture was incubated for 0.5–2 h at 37 °C, 2.5 mL of 10% w/v SDS was added, and the resultant mixture was incubated for 0.5–2 h at room temperature on a shaker (LMS Co. Ltd., Tokyo, Japan). Bacteriolysis within the whole sheath was confirmed with differential interference contrast optics and a light microscope. To further prepare protein-free sheath remnants, we collected the LES-treated sheath materials after they were washed twice by centrifugation in UPW, then treated them with 50–100 μg/mL proteinase K (Nacalai Tesque, Kyoto, Japan) at 37 °C for 12 h (hereafter, LES/ProK treatment). Then the specimens were washed in UPW at least six times. Proteolysis was confirmed by silver staining of the SDS-PAGE gel after separation of the LES-treated and LES/ProK-treated specimens as described previously (Kunoh et al., 2016a, b).

2.3. Sample preparation to screen sheath remnants for sorbed metallic and nonmetallic elements

The 48 elements (Supplementary Table S1) that were selected for the water solubility of available salts, for except $PdCl_2$ and $SbCl_3$, were screened. The respective experimental units (Fig. 2 and Supplementary Figs. S1–7) consisted of tests with six metallic or nonmetallic test compounds, an untreated control to show the background level of element detection, and a positive control using Fe salts such as $FeCl_2$, $FeCl_3$, $Fe(NO_3)_3$ or $Fe(SO)_4$, which were selected for examining the possible influence of anions on sorption behavior against the sheath remnants. The UPW suspensions of the LES/ProK-treated sheath remnants were equally dispensed into eight tubes, then mixed with 1/8 volume of a 100 mM solution of independently dissolved metallic or nonmetallic test salts (final concentration of each: 12.5 mM). The resultant mixtures were incubated for 12–17 h at room temperature on the same shaking mixer as above. For these treatments, all solutions of the water-soluble salts were prepared with UPW, but those of acid-soluble $PdCl_2$ and $SbCl_3$ were prepared with 1.5 N HCl. After incubation, the respective specimens were collected and washed with UPW by centrifugation at least six times. For the $PdCl_2$ or $SbCl_3$ treatments, the specimens were collected and washed with 1.5 N HCl at least six times to wash out excess unbound salts before the six UPW washings. The washed specimens were freeze-dried and subjected to XRF, XRD, and electron microscopy analyses for confirming the degree of sorption of the test elements onto sheath remnants.

2.4. XRF analysis

The freeze-dried specimens were packed into a small aluminum pan to detect the sorbed elements in an Orbis Micro X-ray Fluorescence (XRF) analyzer (AMETEK, Berwyn, PA, U.S.A.). Quantitative data for the target element in the specimen were expressed as

atomic percentage (hereafter atomic %), defined as the percentage of the theoretical intensity of characteristic x-ray fluorescence from target element per a total characteristic x-ray fluorescence from all constitutive elements, which is calculated using physical constants and instrumental parameters by the fundamental parameter method (Kataoka, 1989). Atomic % of any detected element with the standard error was expressed as the mean value and an error bar based on 10 spots.

2.5. Electron microscopic imaging, EDX elemental mapping, and ED analysis

The freeze-dried specimens were suspended in 99.5% ethanol using an ultrasonicator (Branson 2510, Danbury, CT, USA) and filter-collected through a microgrid, then air-dried. HAADF images were obtained with a TEM (JEOL 2100F, Tokyo, Japan), and elemental mapping was done with the TEM equipped with a CEOS Cs corrector (for spherical correction) and an EDX detector (JED-2100T, JEOL). At least three runs were accumulated for the respective EDX images. ED patterns were obtained by employing the electron diffraction mode of TEM.

2.6. XRD analysis

To examine crystallinity of the specimens sorbing Ag, Cu, or Pt, we obtained XRD patterns of freeze-dried specimens using an RINT-2500HF X-ray generator (Rigaku, Tokyo, Japan) with Cu-Kα radiation (voltage: 40 kV; current: 200 mA) as described previously (Suzuki et al., 2015). The freeze-dried specimens were fixed on a zero background sample holder and scanned continuously from 10° to 90° (2θ value) at a rate of 3°/min. The XRD pattern of the zero background sample holder was also measured.

2.7. FT-IR spectroscopy

To examine chemical bonds in the specimens sorbing Ag, Cu, or Pt, we recorded Fourier transform infrared (FT-IR) spectra of the specimens at room temperature using a KBr method and a JASCO FT/IR-4200 spectrometer with a TGS detector (Hachioji, Tokyo, Japan). A total of 64 detector readings were accumulated at a spectral resolution of 4 cm^{-1}. Before the measurement, the washed specimens were heated at 300 °C using an oven (KDF S-90, Denken-Highdental Co., Ltd., Kyoto, Japan) for 2 h for eliminating chemically bonded H_2O molecules after the LES/ProK-treated sheath remnants were mixed with the respective metallic solutions for 12–26 h and washed with UPW. The heated specimens (~8 mg) were pressed into a 10-mm-diameter pellet. Two separate sets of control specimen were measured to assess random vibrations.

3. Results and discussion

3.1. Screening of metallic and nonmetallic elements sorbed by the LES/ProK-treated sheath remnant

The freeze-dried LES/ProK-treated sheath remnant (referred to as original sheath remnant) was a whitish nanofibril aggregate (Fig. 1a). After incubation of the sheath remnant with the respective element solutions, some remnants remained whitish (Fig. 1c, g, j, k, and n), while others changed to light to dark brownish (Fig. 1b, d, and k), light greenish (Fig. 1f), light pinkish (Fig. 1e and h), light yellowish (Fig. 1l), or blackish (Fig. 1m).

To examine the quantitative sorption degree of each element, we analyzed the specimens with XRF after mixing them with the solutions of the respective test elements. Remarkable levels of P, S, Cl, and Ca, which arguably were ascribed to components of the surrounding medium, were detected in the original sheath remnant before mixing with the solutions (Fig. 2). This result agrees quite well with the detection of these elements in the whole sheaths (Furutani et al., 2011; Ishihara et al., 2014; Kennedy et al., 2003; Sakai et al., 2010). Notably, a small peak of Fe was also detected in the original sheath remnant (Fig. 2A, none), indicating that Fe (2–3 atomic %) was deposited in the immature sheaths within 2 days culture in MSVP. As was reported (Chan et al., 2009; Seder-Colomina et al., 2013), such a high amount of Fe likely exists as iron oxyhydroxides in the sheath remnant.

The XRF patterns of an experimental set of six elements (Ag, Au, Co, Cu, Pt, and Zn) are illustrated in Fig. 2 as an example; those for the other 41 elements are shown in Supplementary Figs. S1–7. The XRF patterns showed prominent peaks corresponding to the respective test elements plus the positive control Fe (Fig. 2A), being consistent with those of Fe in the *Leptothrix* whole sheaths that were incubated in the medium containing $FeSO_4$, $Fe_2(SO_4)_3$, or $FeCl_2$ solution (Kunoh et al., 2016b) or Fe(0) powder (Kunoh et al., 2016a).

The atomic % in the specimens varied among test elements: ~55% (Au), ~44% (Ag), ~31% (Pt), ~25% (Cu), ~20% (Fe), and ~15% (Co, Zn) (Fig. 2B). The order of affinity of these metals for the nanofibrils agreed quite well with the concept of "soft cations", according to Pearson's hard and soft acids and bases theory (Pearson, 1963) (hereafter referred to as HSAB theory). The fact that Au has the highest atomic % was not unexpected, as it is known to readily bind various types of natural or synthetic polymers that have a terminal NH_2 group such as chitosan (Daniel and Astruc, 2004; Vo et al., 2014). When other elements were examined (Supplementary Figs. S1–7), prominent peaks and notable atomic % (x) of the respective elements were unexceptionally detected in the XRF patterns. Among these elements, Zr (Supplementary Fig. S4B), Ru and Ti (Supplementary Fig. S5B), and Rh (Supplementary Fig. S6B) showed a high sorption degree ($x \geqq 35\%$). Based on the atomic %, the sorption degree of the test elements to the sheath remnants was color-mapped in the periodic table of Fig. 3. Higher sorption ($x \geqq 35\%$) to the remnant was seen for Ti, Y, Zr, Ru, Rh, Ag, and Au, besides Fe (red-colored), while the blue-colored elements had relatively lower sorption ($x < 15\%$) and other elements had intermediate sorption (green $15\% \leqq x < 25\%$; yellow $25\% \leqq x < 35\%$). Considering the fact that sheath-encased cells were lysed and all proteins hydrolyzed in the sheath biomass (Kunoh et al., 2016b), it is reasonable to categorize this sorption of elements by this biomass as biosorption (Davis et al., 2003). The atomic % of Fe detected in the specimens that were treated with Fe(II) or Fe(III) salts ranged from 20 to 35% regardless of the salt types (Fig. 2, Supplementary Figs. S1–7), suggesting that the cationic Fe, but not anions of the test salts, may be closely associated with the sorption and that the valency of the elements does not seem to be directly associated with the degree of sorption.

For further detailed analyses by XRD and electron microscopy, we selected Ag, Pt, and Cu (all are classified as soft cations in the HSAB theory) as representative of high (atomic % $x \geqq 35\%$), intermediate ($25\% \leqq x < 35\%$), and low ($15\% \leqq x < 25\%$) sorption groups (Fig. 3), respectively.

3.2. TEM imaging, element distribution, crystallinity of sheath remnants sorbing Ag, Cu, and Pt

In HAADF images of the original sheath remnant before treating with the test solutions, a bundle-like structure ~5 μm wide was observed on a microgrid (Fig. 4Aa), consistent with our previous observation (Kunoh et al., 2016b). This structure is an aggregation of nanofibrils as seen in Fig. 5A; hence, we refer to it hereafter as a nanofibril aggregate. In the EDX distribution maps, C (~89% atomic

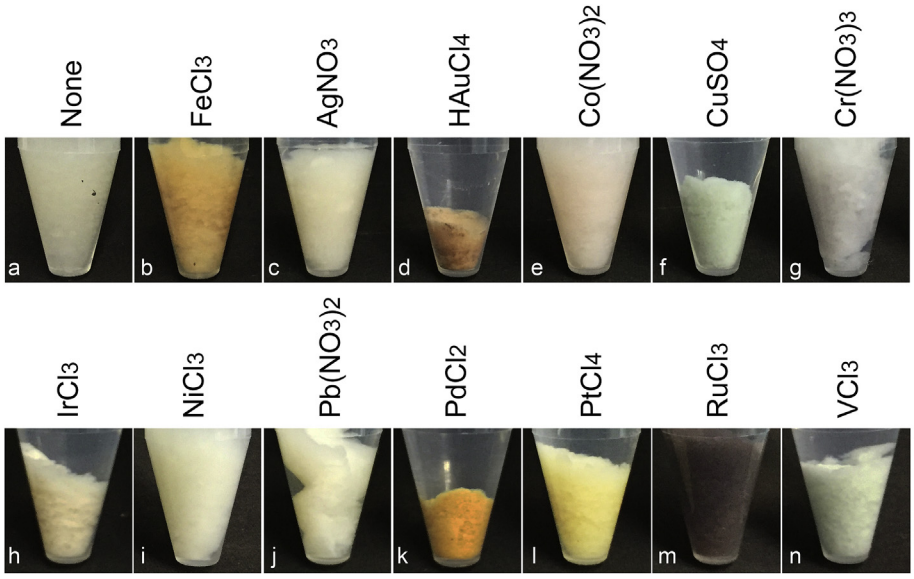


Fig. 1. Visual appearance of LES/ProK-treated sheath remnants after sorbing 13 test metallic elements. The original sheath remnant (i.e., not mixed with a test chemical solution) (a) was whitish. After incubation with the respective element solutions, some remnants remained whitish (c, g, i, j, n); others turned light to dark brownish (b, d, k), light greenish (f), light pinkish (e, h), light yellowish (l), or blackish (m).

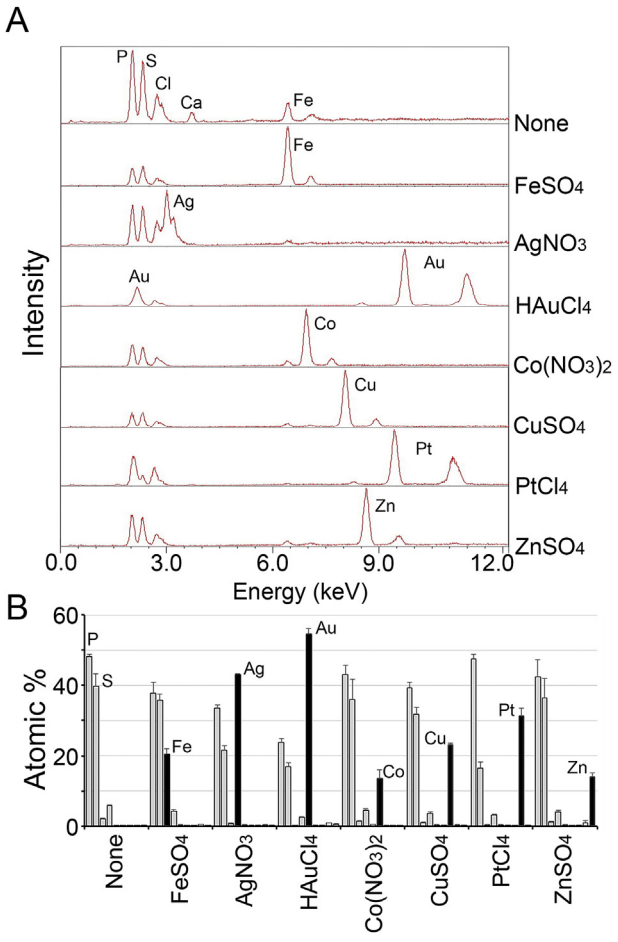


Fig. 2. XRF spectrographs (A) and atomic percentages (B) of six elements (Ag, Au, Co, Cu, Pt and Zn) tested for sorption to the sheath remnant and the positive Fe-sorbed control. A: Prominent peaks of specific energy for the respective elements were detected in addition to notable levels of P, S, Cl, Ca, and Fe. B: The atomic % of the sorbed elements varied among the six test elements, as did the positive control Fe (~20%): ~55% (Au), ~44% (Ag), ~31% (Pt), ~25% (Cu), and ~15% (Co, Zn).

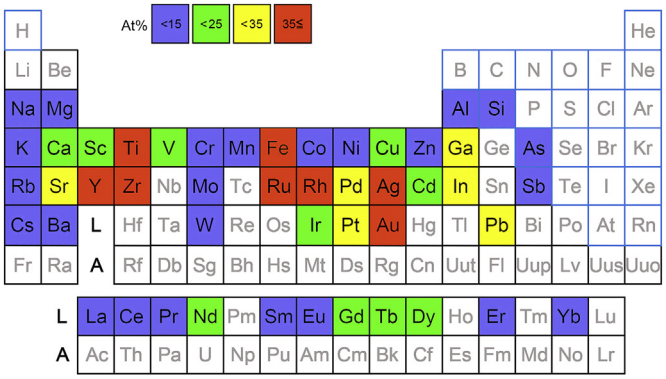


Fig. 3. Color map of the periodic table shows the degree of sorption of the 47 test elements in the sheath remnants based on their atomic % (x). The higher sorption ($x \geqq 35\%$) was found for Ti, Y, Zr, Ru, Rh, Ag, and Au besides Fe; the blue-colored elements had relatively lower sorption ($x < 15\%$). Other elements had intermediate sorption ($15\% \leqq x < 25\%$, green; $25\% \leqq x < 35\%$, yellow). (For interpretation of the references to colour in this figure legend, the reader is referred to the web version of this article.)

%), N (~3.2%), and O (~4.9%) were the major elements (Fig. 4Ab-d), plausibly reflecting that the nanofibril aggregate is composed of C-rich organic materials, in line with an earlier supposition that the sheath fibrils consist of high-molecular-weight hetero-polysaccharide–protein complexes (Emerson and Ghiorse, 1993b) and that the sheath material is constructed from a structural glycoconjugate that is a straight-chained amphoteric hetero-polysaccharide linked with glycine and cysteine (Takeda et al., 2005, 2010). TEM observation at a high magnification (Fig. 4Ae) and the ED pattern (Fig. 4Af) demonstrated that the nanofibril aggregate was nearly in an amorphous state. This state is similar to the amorphous state of the fibrous network of *L. ochracea* sheath surface previously detected by TEM and ED analyses (Suzuki et al., 2011).

In the $AgNO_3$-treated sheath remnants, fine particles of varied sizes were scattered on a nanofibril aggregate (Fig. 4Ba, arrowheads). EDX demonstrated that these particles contained Ag

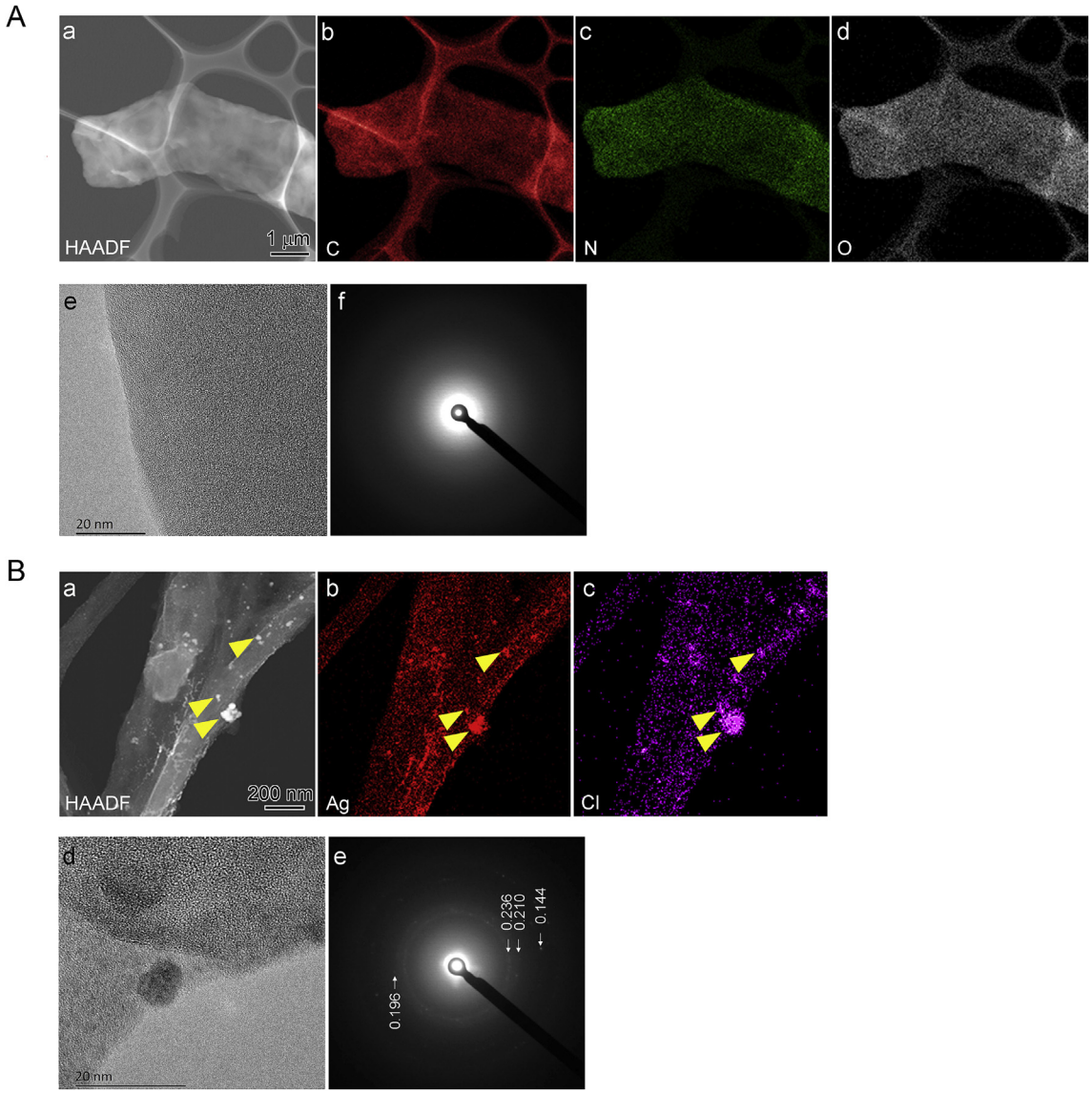


Fig. 4. HAADF images, EDX element distribution patterns, and ED pattern of the original sheath remnant before mixing with solutions of test elements (A) and after mixing with $AgNO_3$ (B). A: HAADF (a) image of aggregated nanofibrils. Area EDX maps show nearly homogeneous distribution of C (b), N (c), and O (d) throughout the nanofibrils. Highly enlarged TEM image shows the amorphous state of the nanofibril matrix (e), and an ED pattern with no distinct diffraction spots (f) also supports that state. B: HAADF (a) image of aggregated nanofibrils. Area EDX maps showing distribution of Ag (b) and Cl (c). Note that particles (arrowheads) in the HAADF image (a) show strong signals of Ag (b, arrowheads) and Cl (c, arrowheads). Highly enlarged TEM image showing amorphous state of the nanofibril matrix (d) and ED pattern with no distinct diffraction spots (e). d-Spacing values, 0.236, 0.210, and 0.144 nm, which corresponded to Ag (111), (020), and (020), respectively, and 0.196 nm, which corresponded to AgCl (220), were obtained from the ED pattern (f).

(Fig. 4Bb). The diffraction indices of Ag, 0.236 nm, 0.210 nm, and 0.144 nm, and AgCl, 0.196 nm, were calculated from the ED pattern and indicated the co-existence of the metallic Ag and AgCl (Fig. 4Be), consistent with the nearly same distribution patterns of Ag and Cl (Fig. 4Bc). The faintish halo area with no distinct diffraction spots (Fig. 4Be) suggests that a small amount or low crystallinity of Ag and AgCl might be present, which is supported by the homogeneous-looking matrix of the sheaths in an enlarged TEM image (Fig. 4Bd).

In the $CuSO_4$-treated sheath remnants, several nanofibrils 5–10 nm thick projects from the nanofibril aggregate in the HAADF image in Fig. 5Aa (arrowhead); apparently, the bundle-like structure (Fig. 4A and B) is an aggregation of nanofibrils. The distribution map (Fig. 5Ab) showed that the distribution of Cu was nearly homogeneous throughout the aggregate. An enlarged TEM image (Fig. 5Ac) and ED image with no distinct diffraction spots (Fig. 5Ad) indicated that the treatment of the nanofibrils with $CuSO_4$ solution did not greatly influence the nearly amorphous state of the nanofibril aggregate.

For the $PtCl_4$-treated sheath remnants, the TEM (Fig. 5Ba and b) and ED pattern, which had no distinct diffraction spots (Fig. 5Bc), demonstrated the nearly amorphous state of the nanofibril aggregate. Although the Pt signal was not strong enough for acquiring a distribution map, spot analysis enabled the detection of prominent Pt peaks at two spots on the nanofibril aggregate (Fig. 5Bd, e), even though the spots were electron-dense (Fig. 5Bb, P1) and amorphous-looking (Fig. 5Bb, P2), suggesting that the Pt distribution was also nearly homogeneous in the nanofibril aggregation. Cu peaks are considered to be noise signals from the Cu-mesh used for specimen preparation.

XRD analyses did not show any peaks characteristic of Ag, Cu, and Pt in sheath remnants that were mixed with these solutions

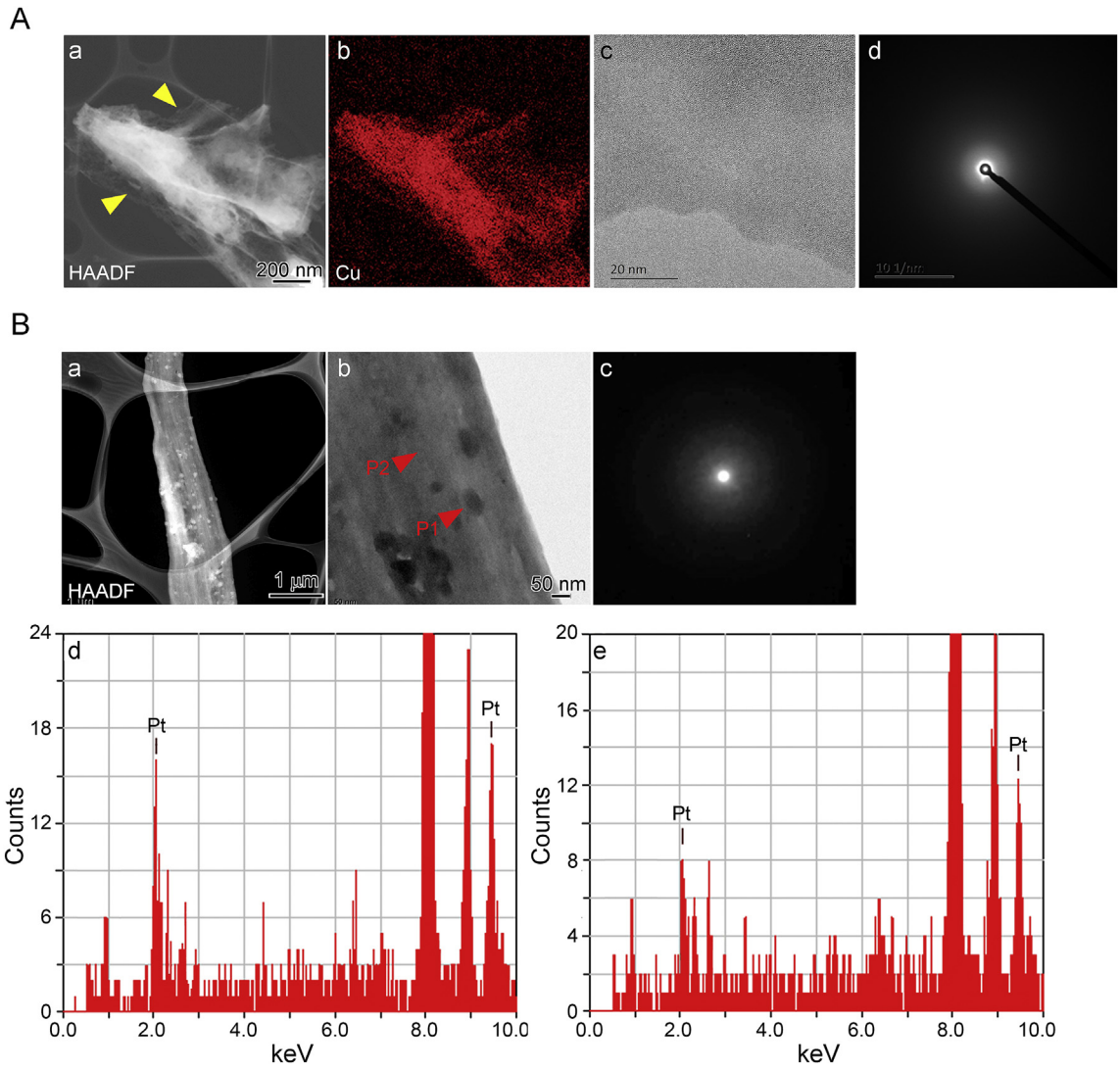


Fig. 5. HAADF images, EDX analysis patterns, and ED pattern of the sheath remnants after mixing with $CuSO_4$ (A) and $PtCl_4$ (B). A: HAADF (a) image of aggregated nanofibrils. Note the constituent nanofibril 5–10 nm wide (arrowheads). Area EDX maps show nearly homogeneous distribution of Cu (b) throughout these same nanofibrils. Highly enlarged TEM image of a nanofibril aggregate shows the amorphous state of the matrix (c) and ED pattern with no distinct diffraction spots (d) also proves that state. B: TEM image of a nanofibril aggregate (a) and highly enlarged TEM image showing electron-dense spots (b, arrowheads) in the amorphous-looking matrix. (c) EDX pattern with distinct diffraction spots that was acquired from an electron-dense spot (b, P1). (d, e) EDX spectra acquired from electron-dense spot (b, P1) and amorphous-looking spot (b, P2), respectively, showing prominent Pt peaks.

(Fig. 6A). However, detailed analysis of the slopes detected using different settings than used for Fig. 6A revealed small peaks corresponding to metallic Ag and AgCl that could plausibly be ascribed to binding of Ag^+ from $AgNO_3$ and Cl^- from a medium component (Fig. 6B), consistent with the EDX and ED analyses (Fig. 4Bb, c, f). These peaks were not detected in Fig. 6A, perhaps because the amount of this salt is quite small and present in a low crystalline state. Shallow slopes without any peaks in Fig. 6A spectra suggest that these cationic elements plausibly bound ionically with anionic functional groups of organics constituting the amorphous nanofibril aggregate. However, although the previous ED indices suggest the presence of metallic Ag and AgCl, the sorption forms of Ag in sheath remnants need to be studied in more detail, because the presence of mixture of multiple forms cannot be ruled out. Although a reduction of Ag^+ to Ag(0), probably followed by the formation of metallic Ag-nanoparticles, is inferred from the present data, further detailed study is certainly needed to explain the occurrence of metallic Ag in sheath remnants.

3.3. Analysis of FT-IR spectra recorded for sheath remnants sorbeing Cu, Ag, and Pt

Shown in Fig. 7 are the FT-IR spectra for the specimens sorbing Cu, Ag, and Pt, as well as for the control specimen (= the LES/ProK-treated sheath remnants before mixing with the metallic solutions). For every specimen, a broad band was centered at around 3150 cm^{-1} at the wavenumber region of 3700–2500 cm^{-1} (Fig. 7a-d, two-way dotted arrow). The bands appearing in this wavenumber region could be due to the surface hydroxyl groups and physisorbed water molecules (Jitianu et al., 2002; Nakamoto, 1997). Other bands were observed at 2920 and 2850 cm^{-1} (Fig. 7, arrowheads), which are assigned to the C–H stretching vibrations of organic components in the specimens (Jitianu et al., 2002; Nakamoto, 1997). The bands at 3390–3140 cm^{-1} (Fig. 7, two-way open arrows) were observed in specimens with sorbed metals but scarcely in the control specimen. Notably, bands at 3600–3570 cm^{-1} (Fig. 7, two-way solid arrows) were seen in

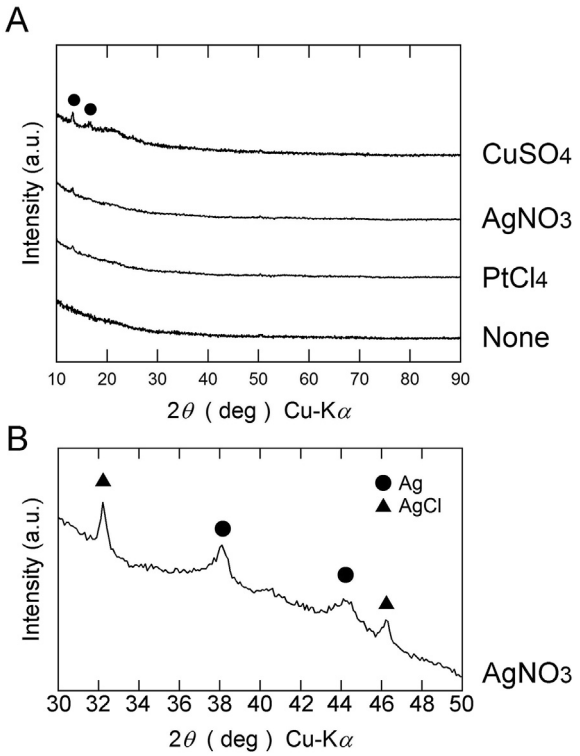


Fig. 6. XRD patterns of sheath remnants before (None) and after mixing with $CuSO_4$, $AgNO_3$, or $PtCl_4$ (A). No prominent characteristic peaks were detected after mixing, similar to those of untreated specimens (None), except for two unidentified peaks (black circles). (B) More detailed XRD pattern obtained from a separate sheath remnant after mixing with $AgNO_3$. Two peaks (triangles) correspond to AgCl; other peaks (circles) correspond to metallic Ag.

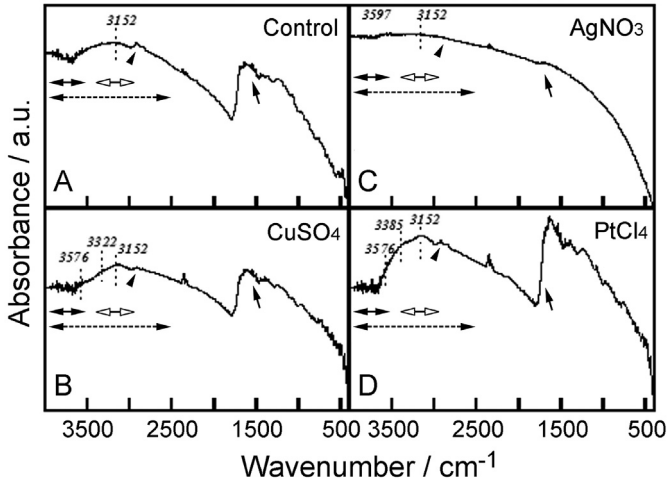


Fig. 7. FT-IR spectra of sheath remnants before (control) and after mixing with $CuSO_4$, $AgNO_3$, or $PtCl_4$: (A) untreated control, and (B) Cu-, (C) Ag-, and (D) Pt-sorbed specimens. Two-way dotted arrows show the plausible existence of surface hydroxyl groups and physisorbed water molecules. Arrowheads: assigned C–H stretching vibrations of organic components. Two-way solid arrows: O–H stretching vibrations of OH coordinating these metallic ions. Two-way open arrows: plausibly due to the overtone of the bending vibration at 1650 cm^{-1}.

control and metal-sorbed specimens, although they were not so clear in Ag-sorbed specimen (Fig. 7C). Their absorbance increased toward 3600 cm^{-1} from 3570 cm^{-1} in control specimens, slightly different from that of metal-sorbed specimens. Because the spectra of control specimen were quite similar in two separate measurements, we judged that the disputant bands were not due to random vibrations.

Considering the band from the AlMgCuOH vibration detected in Cu-sorbed bentonite at 3514 cm^{-1}, the bands at 3600–3570 cm^{-1} in the Cu-, Ag-, and Pt-sorbed specimens plausibly correspond to the O–H stretching vibrations of OH coordinating these metallic ions. On the other hand, the bands at 3390–3140 cm^{-1} could be due to the overtone of the bending vibration of H_2O at 1650 cm^{-1} (Eren and Afsin, 2008; Madejová, 2003). These results suggest that the metallic ions were not only deposited on the surface of the specimens, but they were also chemically bound to the organic constituents via OH. According to Nieboer and Richardson (1980), Cu, Ag, and Pt are all classified as "soft cations" of the HSAB theory, which preferentially bind O-, N-, or S-containing functional groups (e.g., carboxyl, phosphate, hydroxyl, amino, thiol) (Gok and Aytas, 2014). Although the present study does not provide any clues for these possibilities, further investigation concerning the binding mode of the metallic ions and functional groups in nanofibrils may open new approaches to verify the encrustation of sheath material with inorganics.

In aquatic systems, complex interactions occur between various metal-complexing agents with microbes and/or their constituent organic polymers (Ferris et al., 1989). The present TEM, EDX, ED, XRD, and FT-IR analyses demonstrated that aqueous-phase Ag, Cu, and Pt were evidently sorbed, by so-called biosorption, to amorphous nanofibrils that make up the basic skeleton of protein-free sheath remnants, providing evidence that the exopolymer nanofibrils of SP-6 have the potential to sorb a variety of metallic and nonmetallic elements, especially so-called transition elements, regardless of their valency (Fig. 3). The sheaths of *Leptothrix* spp. and *Sphaerotilus natans*, another aquatic Fe-oxidizing bacterium, were reported to have a high affinity for a variety of metal cations such as Fe, Zn, and Pb (Boonfueng et al., 2009; Chan et al., 2009; Furutani et al., 2011; Kunoh et al., 2016a, b; Nelson et al., 1999, 2002; Seder-Colomina et al., 2013). Although the present results suggest that such a high affinity could at least partially depend on the functional groups in the sheath skeleton materials, the secondary role of Fe complexes (Fe oxides and/or Fe oxyhydroxides) which exist in the immature sheaths should not be ruled out, because they were reported to be efficient sorbents for heavy metals and radionuclides (Seder-Colomina et al., 2013).

The NH_2- and OH-groups in chitosan, a polysaccharide composed of β-(1–4)-linked *N*-acetyl glucosamine, jointly work to trap diverse metal ions from aqueous environments (Barakat, 2011; Kyzas and Bikiaris, 2015; Ogawa and Oka, 1993; Shinde et al., 2013; Vo et al., 2014; Zhang et al., 2016). For example, chitosan, a naturally occurring biopolymer, has a strong affinity with transition metal ions such as Cu(II), Fe(III), La(III), Mo(VI) and Zr(IV) and can form a complex with these ions to take up inorganic arsenic anions such as As(V) in an aqueous medium (Shinde et al., 2013). The present FT-IR data (Fig. 7) suggested that the OH-group in sheath remnants could play a role in binding metallic ions. Although the molecular structure of chitosan is not comparable to the basic components of organic polymers in the sheath remnants, chitosan will be a good reference material to verify the role of OH- and NH_2-groups in the sorption capability of the sheath polymers, which have aminosugars with a terminal NH_2 group (Emerson and Ghiorse, 1993a; Takeda et al., 2005, 2010).

4. Conclusions

Organic polymers can play important roles in ecosystems by accumulating biologically important elements, and microbial polymers can scavenge iron oxide particles and induce

crystallization of unexpected phases (Chan et al., 2004). A number of earlier works reported that extracellular polymeric substance (= exopolymer nanofibrils in this paper) excreted from a variety of bacteria including *Leptothrix* spp., exhibited a high affinity for diverse metallic cations (Boonfueng et al., 2009; More et al., 2014). To date, metal encrustation of the *Leptothrix* sheaths has been considered to occur through the interaction of the functional groups of their constituent organics with aqueous-phase inorganics (Emerson and Ghiorse, 1993a; Furutani et al., 2011; Spring 2006; Takeda et al., 2005). According to earlier works (Emerson and Ghiorse, 1993a; Takeda et al., 2005, 2010), the basic organic skeleton of *Leptothrix* sheaths consists of polysaccharide–protein complexes containing glycine, cysteine, galactosamine, glucosamine and uronic acids. Although the present study failed to show the mode of sorption of the nanofibrils of the *Leptothrix* sheaths, we infer that at least the NH_2- and OH-groups in the galactosamine and/or glucosamine units of the nanofibrils could play an important role in such chelating actions. The important issues to be studied in more detail are (i) the mode of interaction between reactive surfaces of the sheath nanofibrils and the test elements and (ii) the influence of factors such as pH, nanofibril quantity, matrix parameters, and ionic strength that influence the biosorption (Seder-Colomina et al., 2013). To further understand the mode of sorption, we are now investigating whether blocking these functional groups in the nanofibrils interferes in their sorption degree for various metal ions.

We expect that the present study provides an additional approach to create novel filtering materials for recovering and recycling useful and/or hazardous elements from the aquatic environment. These and other potential industrial applications of the Fe-encrusted *Leptothrix* sheaths such as lithium-ion battery anode material, catalyst, porcelain pigment (Kunoh et al., 2015), and starting materials to create novel complexes (Zhang et al., 2012) illustrate the great cost-effective usefulness of these remarkable natural sheaths.

Acknowledgments

We thank Ms. Keiko Toyoda for technical support. We also acknowledge Dr. Beth E. Hazen for reviewing and editing the English in the manuscript. This study was financially supported by JST-CREST (2012–2017) (J. T.).

Appendix A. Supplementary data

Supplementary data related to this article can be found at http://dx.doi.org/10.1016/j.watres.2017.05.003.

References

Barakat, A.M., 2011. New trends in removing heavy metals from industrial wastewater. Arab. J. Chem. 4 (4), 361–377. http://dx.doi.org/10.1016/j.arabjc.2010.07.019.

Bhat, V., Rao, P., Patil, Y., 2012. Development of an integrated model to recover precious metals from electronic scrap - a novel strategy for e-waste management. Procedia Soc. Behav. Sci. 37, 397–406. http://dx.doi.org/10.1016/j.sbspro.2012.03.305.

Boonfueng, T., Axea, L., Yee, N., Hahn, D., Ndiba, P.K., 2009. Zn sorption mechanisms onto sheathed *Leptothrix discophora* and the impact of the nanoparticulate biogenic Mn oxide coating. J. Colloid Interface Sci. 333 (3), 439–447. http://dx.doi.org/10.1016/j.jcis.2009.02.033.

Chan, C.S., de Stasio, G., Welch, S.A., Girasole, M., Frazer, B.H., Nesterova, M.V., Fakra, S., Banfield, J.F., 2004. Microbial polysaccharides template assembly of nanocyrstal fibers. Science 303 (5664), 1656–1658. http://dx.doi.org/10.1126/science.1092098.

Chan, S.C., Fakra, C.S., Edwards, C.D., Emerson, D., Banfield, F.J., 2009. Iron oxyhydroxide mineralization on microbial extracellular polysaccharides. Geochim. Cosmochim. Acta 73 (13), 3807–3818. http://dx.doi.org/10.1016/j.gca.2009.02.036.

Cruz Viggi, C., Pagnanelli, F., Cibati, A., Uccelletti, D., Palleschi, C., Toro, L., 2010. Biotreatment and bioassessment of heavy metal removal by sulphate reducing bacteria in fixed bed reactors. Water Res. 44 (1), 151–158. http://dx.doi.org/10.1016/j.watres.2009.09.013.

Daniel, M.C., Astruc, D., 2004. Gold nanoparticles: assembly, supramolecular chemistry, quantum-size-related properties, and applications toward biology, catalysis, and nanotechnology. Chem. Rev. 104 (1), 293–346. http://dx.doi.org/10.1021/cr030698+.

Davis, T.A., Volesky, B., Mucci, A., 2003. A review of the biochemistry of heavy metal biosorption by brown algae. Water Res. 37 (18), 4311–4330. http://dx.doi.org/10.1016/S0043-1354(03)00293-8.

Emerson, D., Ghiorse, W.C., 1992. Isolation, cultural maintenance, and taxonomy of a sheath-forming strain of *Leptothrix discophora* and characterization of manganese-oxidizing activity associated with the sheath. Appl. Environ. Microbiol. 58 (12), 4001–4010.

Emerson, D., Ghiorse, W.C., 1993a. Ultrastructure and chemical composition of the sheath of *Leptothrix discophora* SP-6. J. Bacteriol. 175 (24), 7808–7818.

Emerson, D., Ghiorse, W.C., 1993b. Role of disulfide bonds in maintaining the structural integrity of the sheath of *Leptothrix discophora* SP-6. J. Bacteriol. 175 (24), 7819–7827.

Emerson, D., Fleming, E.J., McBeth, J.M., 2010. Iron-oxidizing bacteria: an environmental and genomic perspective. Annu. Rev. Microbiol. 64 (1), 561–583. http://dx.doi.org/10.1146/annurev.micro.112408.134208.

Eren, E., Afsin, B., 2008. An investigation of Cu(II) adsorption by raw and acid-activated bentonite: a combined potentiometric, thermodynamic, XRD, IR, DTA study. J. Hazard. Mater. vol. 151 (2–3), 682–691. http://dx.doi.org/10.1016/j.jhazmat.2007.06.040.

Ferris, F.G., Schultze, S., Witten, T.C., Fyfe, W.S., Beveridge, T.J., 1989. Metal interactions with microbial biofilms in acidic and neutral pH environments. Appl. Environ. Microbiol. 55 (5), 1249–1257.

Furutani, M., Suzuki, T., Ishihara, H., Hashimoto, H., Kunoh, H., Takada, J., 2011. Initial assemblage of bacterial saccharic fibrils and element deposition to form an immature sheath in cultured *Leptothrix* sp. strain OUMS1. Minerals 1 (1), 157–166. http://dx.doi.org/10.3390/min1010157.

Ghiorse, W.C., 1984. Biology of iron- and manganese-depositing bacteria. Annu. Rev. Microbiol. 38, 515–550.

Gok, C., Aytas, S., 2014. Chapter 16. Biosorption of uranium and thorium by biopolymers. In: Fanun, Monzer (Ed.), Role of Colloidal Systems in Environmental Protection, first ed. Elsevier, Amsterdam, ISBN 978-0-444-63283-8, pp. 363–395.

Han, R., Li, H., Li, Y., Zhang, J., Xiao, H., Shi, J., 2006. Biosorption of copper and lead ions by waste beer yeast. J. Hazard Mater. 137 (3), 1569–1576. http://dx.doi.org/10.1016/j.jhazmat.2006.04.045.

Inoue, M., Nakano, T., Yamasaki, A., 2015. Fabrication of precious metals recovery materials using grape seed-waste. Sustain. Mater. Technol. 3, 14–16. http://dx.doi.org/10.1016/j.susmat.2014.11.005.

Ishihara, H., Suzuki, T., Hashimoto, H., Kunoh, H., Takada, J., 2013. Initial parallel arrangement of extracellular fibrils holds a key for sheath frame construction by *Leptothrix* sp. strain OUMS1. Minerals 3, 73–81. http://dx.doi.org/10.3390/min3010073.

Ishihara, H., Hashimoto, H., Taketa, E., Suzuki, T., Mandai, K., Kunoh, H., Takada, J., 2014. Silicon-rich iron oxide microtubular sheath produced by an iron-oxidizing bacterium, *Leptothrix* sp. strain OUMS1, in culture. Minerals 4 (3), 565–577. http://dx.doi.org/10.3390/min4030565.

Jitianu, A., Crisan, M., Meghea, A., Rau, I., Zaharescu, M., 2002. Influence of the silica based matrix on the formation of iron oxide nanoparticles in the Fe_2O_3-SiO_2 system, obtained by sol-gel method. J. Mater. Chem. 12, 1401–1407. http://dx.doi.org/10.1039/B110652J.

Kataoka, Y., 1989. Standardless x-ray fluorescence spectrometry (fundamental parameter method using sensitive library). Rigaku J. 6 (1), 33–40.

Kennedy, C.B., Scott, S.D., Ferris, F.G., 2003. Ultrastructure and potential sub-seafloor evidence of bacteriogenic iron oxides from Axial Volcano, Juan de Fuca Ridge, north-east Pacific Ocean. FEMS Microbiol. Ecol. 43 (2), 247–254. http://dx.doi.org/10.1111/j.1574-6941.2003.tb01064.x.

Kunoh, T., Kunoh, H., Takada, J., 2015. Perspectives on the biogenesis of iron oxide complexes produced by *Leptothrix*, an iron-oxidizing bacterium and promising industrial applications for their functions. J. Microb. Biochem. Technol. 7 (6), 419–426. http://dx.doi.org/10.4172/1948-5948.1000249.

Kunoh, T., Hashimoto, H., Suzuki, T., Hayashi, N., Tamura, K., Takano, M., Kunoh, H., Takada, J., 2016a. Direct adherence of Fe(III) particles onto sheaths of *Leptothrix* sp. strain OUMS1 in culture. Minerals 6 (1), 4. http://dx.doi.org/10.3390/min6010004.

Kunoh, T., Hashimoto, H., McFarlane, R.I., Hayashi, N., Suzuki, T., Taketa, E., Tamura, K., Takano, M., El-Naggar, Y.M., Kunoh, H., Takada, J., 2016b. Abiotic deposition of Fe complexes onto *Leptothrix* sheaths. Biol. (Basel) 5 (2), 26. http://dx.doi.org/10.3390/biology5020026.

Kyzas, Z.G., Bikiaris, N.D., 2015. Recent modifications of chitosan for adsorption applications: a critical and systematic review. Mar. Drugs 13 (1), 312–337. http://dx.doi.org/10.3390/md13010312.

Madejová, J., 2003. FTIR techniques in clay mineral studies. Vib. Spectrosc. 31 (1), 1–10. http://dx.doi.org/10.1016/S0924-2031(02)00065-6.

More, T.T., Yadav, J.S.S., Yan, S., Tyagi, R.D., Surampalli, R.Y., 2014. Extracellular polymeric substances of bacteria and their potential environmental applications. J. Environ. Manag. 144 (1), 1–25. http://dx.doi.org/10.1016/j.jenvman.2014.05.010.

Nakamoto, K., 1997. Infrared and Raman Spectra of Inorganic and Coordination Compounds, fifth ed. John Wiley & Sons, Inc., New York, pp. 88–95. http://dx.doi.org/10.1002/9780470405840.

Nelson, Y.M., Lionle, W., Ghiorse, W.C., Shuler, M.L., 1999. Production of biogenic Mn oxides by *Leptothrix discophora* SS-1 in a chemically defined growth medium and evaluation of their Pb adsorption characteristics. Appl. Environ. Microbiol. 65 (1), 175–180.

Nelson, Y., Lion, L.W., Shuler, M.L., Ghiorse, W.C., 2002. Effect of oxide formation mechanisms on lead adsorption by biogenic manganese (hydr)oxides, iron (hydr)oxides, and their mixtures. Environ. Sci. Technol. 36 (3), 421–425. http://dx.doi.org/10.1021/es010907c.

Nieboer, E., Richardson, H.S., 1980. The replacement of the nondescript term 'heavy metals' by a biologically and chemically significant classification of metal ions. Environ. Pollut. Ser. B 1, 3–26.

Ogawa, K., Oka, K., 1993. X-ray study of chitosan-transition metal complexes. Chem. Mater. 5 (5), 726–728. http://dx.doi.org/10.1021/cm00029a026.

Pagnanelli, F., Beolchini, F., Di Biase, A., Veglio, F., 2004. Biosorption of binary heavy metal systems onto *Sphaerotilus natans* cells confined in an UF/MF membrane reactor: dynamic simulations by different Langmuir-type competitive models. Water Res. 38 (4), 1055–1061. http://dx.doi.org/10.1016/j.watres.2003.10.031.

Pearson, R.G., 1963. Physical and inorganic chemistry. J. Amer. Chem. Soc. 85 (22), 3533–3539.

Raoa, N.L., Prabhakara, G., 2011. Removal of heavy metals by biosorption – an overall review. J. Eng. Res. Stud. 2 (4), 17–22.

Sakai, T., Miyazaki, Y., Murakami, A., Sakamoto, N., Ema, T., Hashimoto, H., Furutani, M., Nakanishi, M., Fujii, T., Takada, J., 2010. Chemical modification of biogenous iron oxide to create an excellent enzyme scaffold. Org. Biomole. Chem. 8 (2), 336–338. http://dx.doi.org/10.1039/b919497e.

Seder-Colomina, M., Morin, G., Benezerara, K., Ona-Nguema, G., Pernelle, J.-J., Esposito, G., van Hullebusch, E.D., 2013. *Sphaerotilus natans*, a neutrophilic iron-related sheath-forming bacterium: perspectives for metal remediation strategies. Geomicrobiol. J. 31 (1), 1–12. http://dx.doi.org/10.1080/01490451.2013.806611.

Shinde, R.N., Pandey, A.K., Acharya, R., Guin, R., Das, S.K., Rajurkar, N.S., Pujari, P.K., 2013. Chitosan-transition metal ions complexes for selective arsenic(V) preconcentration. Water Res. 47 (10), 3497–3506. http://dx.doi.org/10.1016/j.watres.2013.03.059.

Spring, S., 2006. The genera *Leptothrix* and *Sphaerotilus*. Prokaryotes 5, 758–777. http://dx.doi.org/10.1007/0-387-30745-1_35.

Suzuki, T., Kunoh, T., Nakatsuka, D., Hashimoto, H., Tamura, K., Kunoh, H., Takada, J., 2015. Use of iron powder to obtain high yields of *Leptothrix* sheaths in culture. Minerals 5 (2), 335–345. http://dx.doi.org/10.3390/min5020335.

Suzuki, T., Hashimoto, H., Ishihara, H., Kasai, T., Kunoh, H., Takada, J., 2011. Structural and spatial associations between Fe, O, and C in the network structure of the *Leptothrix ochracea* sheath surface. Appl. Environ. Microbiol. 77 (21), 7873–7875. http://dx.doi.org/10.1128/AEM.06003-11.

Takeda, M., Makita, H., Ohno, K., Nakahara, Y., Koizumi, J., 2005. Structural analysis of the sheath of a sheathed bacterium, *Leptothrix cholodnii*. Int. J. Biol. Macromol. 37 (1–2), 92–98. http://dx.doi.org/10.1016/j.ijbiomac.2005.09.002.

Takeda, M., Kondo, K., Yamada, M., Koizumi, J., Mashima, T., Matsugami, A., Katahira, M., 2010. Solubilization and structural determination of a glyco-conjugate which is assembled into the sheath of *Leptothrix cholodnii*. Int. J. Biol. Macromol. 46 (2), 206–211. http://dx.doi.org/10.1016/j.ijbiomac.2009.

Vo, K.D.N., Guillom, E., Dupont, L., Kowandy, C., 2014. Influence of Au(III) interactions with chitosan on gold nanoparticle. J. Phys. Chem. C 118 (8), 4465–4474. http://dx.doi.org/10.1021/jp4112316.

Zhang, L., Zeng, Y., Cheng, Z., 2016. Removal of heavy metal ions using chitosan and modified chitosan: a review. J. Mol. Liq. 214, 175–191. http://dx.doi.org/10.1016/j.molliq.2015.12.013.

Zhang, W., Cai, J., Zhang, D., 2012. Preparation and properties of ferrite derived from iron oxidizing bacteria. Chin. Sci. Bull. 57, 2470–2474. http://dx.doi.org/10.1007/s11434-012-5192-1.

Zhao, M., Xu, Y., Zhang, C., Rong, H., Zeng, G., 2016. New trends in removing heavy metals from wastewater. Appl. Microbiol. Biotechnol. 100 (15), 6509–6518. http://dx.doi.org/10.1007/s00253-016-7646-x.